Sensing Water Properties at Precise Depths from the Air

John-Paul Ore and Carrick Detweiler

Abstract Water properties critical to our understanding and managing of freshwater systems change rapidly with depth. This work presents an Unmanned Aerial Vehicle (UAV) based method of keeping a passive, cable-suspended sensor payload at a precise depth, with 95% of submerged sensor readings within ± 8.4 *cm* of the target depth, helping dramatically increase the spatiotemporal resolution of water science datasets. We use a submerged depth altimeter attached at the terminus of a semi-rigid cable as the sole input to a method of controlling the altitude of a UAV. We first model both the system and common environmental disturbances of wind, water, and GPS drift before implementing the system. In field experiments, we compare the precision of our new method to using the UAV's air-pressure altimeter or using UAV-mounted ultrasonic sensors. We find that our new method reduces the standard deviation of depth readings by 75% in winds up to 8 m/s. We also show the step response of the system when transitioning between target depths. Finally we explore the depth-altimeter method with a longer, 8 *m* cable and show that our approach still greatly outperforms previous methods.

1 Introduction

Monitoring shallow surface water systems (< 10 *m*) can be deeply challenging for environmental scientists as boat access is often limited and, even if available, boats, wading or other methods might cause mixing that disrupts the very phenomena the scientists seek to measure. Shallow water systems have important water properties that vary sensitively with small changes in water depth [1], such as temperature, conductivity, dissolved oxygen, and photosynthetically active radiation. These stratified properties are closely linked to the health of ecosystems and are used to predict toxic

John-Paul Ore and Carrick Detweiler
Computer Science and Engineering, University of Nebraska-Lincoln, USA e-mail: {jore, carrick}@cse.unl.edu

algae blooms that threaten drinking water and fisheries, costing billions of dollars worldwide [2, 3], and occuring more frequently due to climate change [4].

Our prior work [5] presents the first Unmanned Aerial Vehicle (UAV) based water sampler and in follow-on work we explored *in-situ* water sensing at different depths with a UAV [6]. The UAV flies above the water while dangling a sensor payload in the water as shown in Figure 1. The sensors used by Water scientists include instruments that require some settling time (often > 3 s) and have existing datasets from static sensors with ≈ 0.25 m resolution in depth. These static sensors are often a collection of data-loggers arranged vertically underwater at a fixed position and left for days or weeks. During our prior experiments, we found that the air pressure sensor altimeter provides insufficiently stable positioning of the sensor in the water column, even when coupled with ultrasonic range finders. This was caused by in part by environmental factors like wind and GPS drift as well as the non-ridged coupling of the vehicle to the water sensor and the dampening effect of the water on the motion of the sensor.

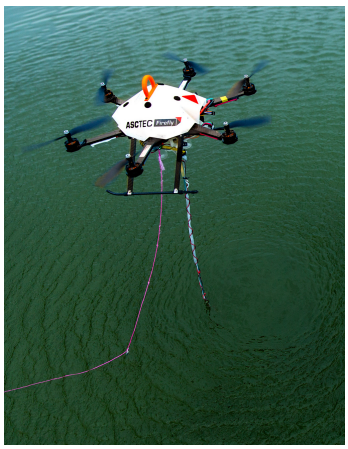

Fig. 1: UAV-system with a passive cable and sensors for measuring water properties at precise depths.

This paper proposes and experimentally evaluates using a precise depth altimeter as input to the UAV altitude controller with the goal of maintaining a more precise depth for the submerged sensor payload. These depth sensors are light ($< 5g$), precise (± 3 mm), and fast (50 Hz), and are already included in many underwater sensor payloads. We first explore the feasibility of this approach in simulation, including modeling both the semi-rigid cable and environmental factors like wind and water, then construct an implementation to validate the approach with field experiments. We demonstrate that using a submerged depth altimeter significantly outperforms the precision of previous methods, reducing the standard deviation of target depth errors from 16.1 cm to 4.2 cm compared with using an altitude estimate from ultrasonic sensors fused with the air-pressure altimeter.

The contributions of this work are:

- A new method to maintain a precise depth for a submerged sensor payload while passively connected by cable to a UAV using only a lightweight depth altimeter, increasing spatiotemporal resolution of water science datasets, without additional payload.
- Field tests of this depth-altimeter approach and comparisons with a UAV's pressure altimeter and an altitude estimate aided by ultrasonic rangers. We compare these approaches using a 3.5 m cable for water depths down to 2.5 m, showing an reduction of target depth error by 75%.
- An initial exploration of using an 8 m cable with a depth altimeter that still improves on previous methods.

2 Related Work

Previous efforts relate to our current work is several ways: either a UAV is used to measure water properties, or autonomous surface vehicles (ASVs) / autonomous underwater vehicles (AUVs) are used to measure water properties, or a UAV makes a pose and altitude estimation in unknown environments, or a UAV has a cable-suspended load. We now discuss each of these related efforts.

Several efforts seek to use UAVs to take water samples and monitor water properties [7, 5, 8, 9, 10, 11]. All of these systems rely on air pressure altimeters as their primary method of maintaining altitude, and like these efforts we seek to sense water properties with a payload connected by a cable, but unlike these works we want to precisely control the depth of the sensor payload. Systems like the Flying Fish [16] maintain persistent observation of water surface properties, but this approach cannot detect water properties inside the water column. Some efforts seek an amphibious UAV that swims underwater [12]. Like this work we are interested in the advantages offered by UAVs to water monitoring, but unlike this work we seek to minimize vertical disturbances to the water column that can take hours to settle. Our previous work presents evidence that sensing by a small, submerged sensor payload (≈ 2 *cm* diameter sensor, 1 *cm* cable) does not cause a mixing disturbance that impacts water temperature measurements [6].

In environmental monitoring, an ASV that monitors water quality was developed by Dunbabin *et al.* [13], while underwater the MARES AUV system samples water quality for long duration at depths up to 100 *m* [14]. Further underwater systems have sought to capture information about water columns using a gliding fish-like robot [15], or by descending to a desired depth like Higgin's Waterbug [1]. Unlike these systems we are interested in the unique advantages a UAV brings to water monitoring, including access to disconnected or difficult to reach water bodies, as well as a UAV's ability to quickly change location.

Several approaches seek to improve altitude estimates for micro UAVs in outdoor environments, including Jain *et al.* [17] who autonomously explored rivers and primarily used specular returns from a rotating laser to estimate the plane of the water. Unlike this work we seek a method that minimizes the payload devoted to non-water-property sensing. Burri *et al.* [18] use a stereo camera and IMU to map and estimate a pose in a previously unknown environment, but these methods have not been demonstrated as effective for altitude estimation in over-water environments, to our knowledge. Our previous work [5] explores the use of fusing downward-facing ultrasonic sensors with air pressure altimeter readings for an altitude estimation over water, and we use this method for comparison in the present work.

Another class of related work pertains to flying with a suspended payload. Although there have been several efforts to model and control a payload suspended from a UAV [19, 20], these method assume the payload can be observed, and do not address a partially submerged cable. We do not attempt to observe or model the cable during flight, but it might be possible to add fiducial markers to the cable that might seen while above water to improve the ability to estimate its depth, although the portion of the cable below the water's surface is barely visible.

3 Technical Approach

This section describes our approach to the problem. Based on our experience, we assume that the biggest obstacles to the problem of using a water depth altimeter as input to the altitude controller of the UAV would be the non-linear dynamics introduced by the submerged cable as wind and GPS drift perturb the system, as well as the impact of the signal delay in measuring and transmitting depth before it can be used by the controller. We start by developing a model for how the cable-connected sensor moves in the water, and then explore the feasibility and initial parameters in simulation.

3.1 System Model and Simulation to Explore Feasibility

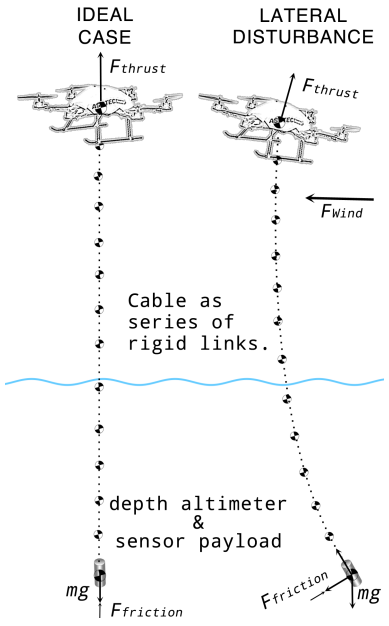

Fig. 2: Model of UAV and suspended cable as a series of rigid links in both ideal conditions and during a lateral disturbance.

We model the UAV-cable system as shown in Figure 2. As shown in the Figure, the UAV is modeled as a point mass and the cable is a series of rigid links, following the modeling approach in [20]. We use Simulink to model two configurations, a ideal and perfectly vertical case, and a laterally disturbed case to model wind and GPS drift.

Modeling the Ideal Case. In the ideal case, the cable is vertical and all forces are parallel to gravity, as the UAV, cable, and depth altimeter move up and down. When the UAV moves up, the sensor payload is directly coupled. When the UAV moves down, the only forces acting on the payload are gravity and resistance from the water. The resistance from the water limits the sensor's descent rate to slower than the vehicle's.

To model the descent rate, we started by experimentally determining the terminal velocity of the sensor in water. We released the sensor at the top of a 3 m vertical test tank ($\approx 25cm$ radius by 4 m tall) and measured the time at which the sensor reached 1 m and 2 m of depth. Using six successive observations, we measured the terminal velocity, v_t, to be 0.54 m/s. We then used the terminal velocity equation:

$$v_t = \sqrt{\frac{2mg}{\rho A C_d}} \tag{1}$$

to calculate the constant ρAC_d, where ρ is the density of water, A is the area in the direction of the movement, and C_d is the drag co-efficient. Using this constant with the mass of the sensor, m, and gravity, g, we solve for the resistive force as a function of velocity:

$$F_{friction} = \frac{1}{2}\rho AC_d v^2 \tag{2}$$

As shown in Figure 2, using $F_{friction}$ we can model how the sensor will descend in water in our simulations. In simulation, decreasing the target depth by < 1 m allowed the submerged sensor to descend fast enough to match the descent of the UAV. Decreasing the target depth by > 1 m requires limiting the descent velocity of the UAV to avoid the UAV outpacing the submerged sensor, causing the UAV to hit the water.

Modeling Lateral Disturbances. Figure 2 also shows the lateral disturbance case from wind or GPS drift. We want to model wind and GPS drift because we believed lateral disturbances could be a critical impediment to our approach. However, simulation indicated an unexpected interaction between the UAV's dynamics and the cable's dynamics that co-incidentally work in opposition to decrease the target depth error during lateral disturbances.

The two opposing dynamics that aid depth precision are caused by 1) during lateral disturbances the UAV pitches and/or rolls, causing less thrust (F_{thrust}) to oppose gravity, resulting in a small decrease in altitude that allows the sensor payload to fall slightly in the water; and 2) the sensor rises slightly as it is pulled laterally and up by a cable attached to the UAV as it translates laterally. For a detailed discussion of UAV dynamics, refer to [21] .

These opposing dynamics are small effects, each on the order of a few centimeters, but together they work to limit the impact of lateral disturbances on the UAV to the depth of the submerged sensor.

Modeling Signal Delay and Sampling Frequency. In addition to lateral disturbances and terminal velocity in water, we also modeled signal delay and sampling frequency of the depth altimeter. We wanted to model signal delay because we know a real system will have some signal propagation delay from the depth altimeter to the embedded system on the UAV and then on to an off-board control station. We wanted to model the sampling frequency to determine a baseline of how fast the depth altimeter would need to be.

In simulation, a sampling rate of at least 10 Hz and a signal delay of at most 100 ms were sufficient to ensure that the system converges to a target depth, with faster sampling rates or smaller signal delays yielding only modest improvements. During simulation, the system could still converge with a slow sampling rate of 1.25 Hz and a long delay of 700 ms, but with significant oscillations.

Key lessons learned from simulation:

- The signal delay from the depth altimeter should not exceed 100 ms.
- The depth altimeter sampling rate should be at least 10 Hz.
- The submerged sensor descends more slowly that the UAV, so the UAV should descend less than 1 m at a time or have descent velocity limits.

- Lateral disturbances, like wind and GPS drift, cause an unexpected interaction between the UAV's dynamics and the cable's dynamics that co-incidentally work in opposition to keep the sensor payload near the same depth, limiting the target depth error during lateral disturbances.

Now that we have modeled and simulated our system, we can use the simulation guidelines for sampling rate, signal delay, and descent velocity to guide our implementation and field tests.

4 Implementation Details

This section describes the system architecture used for the implementation, characterization of the depth altimeter, and a description of the three flight modes.

4.1 System Architecture

Figure 3 shows the architecture of the system used during experiments, consisting of: 1) AscTec Firefly hexrotor UAV; 2) two embedded systems, one on the UAV and another in the water, connected to the UAV by a cable; and; 3) a ground control station laptop.

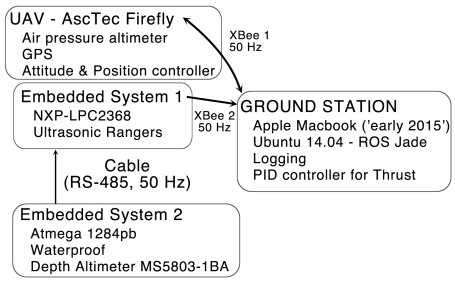

Fig. 3: System Architecture.

The Firefly includes a GPS and air pressure altimeter as well as an onboard controller for attitude and position. We chose the Firefly for overwater experiments because it can fly even if one motor fails. It has a payload capacity of 600 g, flies for 15-20 minutes on one battery, and tolerates winds up to 10 m/s.

The sensor payload installed on the Firefly consists of two embedded systems, the first affixed to the vehicle and the second waterproof system attached to the end of the cable that dangles below the UAV. The first embedded system is installed on the UAV with an NXP-LPC2368 (ARM7TDMI) microprocessor running a control loop at 50 Hz, and has inputs for a variety of water sensors and the depth altimeter and is used to log and transmit realtime readings over radio. The waterproof embedded system consists of an ATmega-1284pb microprocessor and the depth altimeter. The submerged embedded system reads the depth altimeter at 50 Hz, and transmits the depth readings over the dangling data cable using RS-485. The embedded system installed on the UAV receives the depth sensor readings and re-transmits them over a XBee radio to the ground station.

The ground station (Apple Macbook "Early 2015" running virtual machine of Ubuntu 14.04 with ROS Jade for control and logging) has two XBee radio channels:

one to communicate with the AscTec Firefly, and a second to receive a stream of depth readings from embedded system 1 affixed to the undercarriage of the UAV.

In this architecture, we estimate the complete signal delay from the depth altimeter to the control input to be at worst 45 *ms*. The 45 *ms* worst-case signal delay for the depth readings happens if the 50 Hz control loop on the upper embedded system and the 50 Hz ground control PID loop both contribute 20 *ms* and the transmission and processing times add up to 5 *ms*. This worst case estimate is within the 100 *ms* signal delay bound identified during simulation and described in Section 3.1.

4.2 Depth Altimeter Characterization

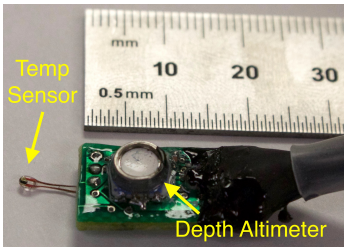

Fig. 4: Depth altimeter embedded system.

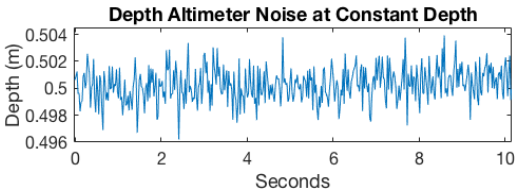

Fig. 5: Depth altimeter steady state error.

For the depth sensor altimeter, we use a Measurement Specialties MS5803-01BA pressure altimeter [22] installed on an embedded system, and shown in Figure 4. By the datasheet, this sensor is water resistant to 100 *m* and has a built-in 24-bit ADC with a 10 *ms* response time, but you must also measure the on-board thermometer to calibrate the altimeter readings, taking an additional 10 *ms*. Since it takes 20 *ms* for one measurement, the MS5803 has a maximum sampling frequency of 50 Hz. The 50 Hz rate is well above the 10 Hz minimum sampling rate suggested by simulation.

To characterize the depth altimeter's steady-state error, we placed it at a fixed depth in a bucket of 22°C water. Figure 5 depicts 10 *s* of readings, and shows a resting background noise of ± 3 *mm*. Because of the MS5803's fast response time, accuracy over the range of depths common in surface freshwater, and small steady-state error, we use this sensor as the ground truth for depth during our field experiments. Further, in order to achieve a vertical resolution of ≈ 0.25 *m* for water science datasets, so that the water properties are comparable with existing datasets, we need a depth altimeter with small steady state error.

Note that changes to ambient air pressure can cause pressure changes in the water, impacting depth readings. For example, the barometric pressure difference of 100 *mbar* across a strong weather front would result in 0.6 *m* difference in pressure readings under water. However, during a 20-minute flight, the total air pressure change is likely to be much smaller than this, and transient air pressure fluctuations

that cause an air altimeter change of ± 2 *m* cause a depth altimeter change of only ± 3 *mm*. This makes sense since water is ≈ 800 times denser than air.

4.3 Flight Modes: Depth Altimeter, Air Pressure Altimeter, Ultrasonic Altimeter

We use three flight modes: depth altimeter mode, air pressure altimeter mode, and ultrasonic altimeter mode. The depth altimeter mode is the new method proposed and implemented in this work, and the air pressure and ultrasonic modes are alternative methods for comparison during experiments.

Depth altimeter mode uses depth readings from the submerged MS5803-1BA sensor at 50 Hz. As shown in Figure 3, the depth signals are transmitted over a RS-485 cable to the embedded system installed on the UAV. From this embedded system, the depth readings are sent over XBee radio 2 to a ground station. On the ground station, the stream of depth readings are Kalman filtered. For the Kalman filter, we assume Gaussian noise in the measurements (characterized in Section 4.2) and we assume a nearly linear state transition function during hover. The filtered readings are used in a 50 Hz PID controller for depth that commands thrust. Finally, the thrust commands are sent by XBee radio 1 to the UAV. In this implementation, the UAV's roll, pitch, and yaw, are governed the UAV's on-board controller. Overall, depth altitude mode controls only thrust by using depth readings sent to an off-board ground station, while the UAV controls roll, pitch, and yaw.

Air pressure altimeter mode uses the UAV's onboard controller for everything: roll, pitch, thrust, and yaw. Air pressure mode uses the UAV's air pressure altimeter, GPS, and an onboard IMU together to create a fused pose estimate. This is the basic 'out-of-the-box' controller.

Ultrasonic altimeter mode uses downward-facing ultrasonic sensors fused with the air-pressure altimeter to form an altitude estimate. To prevent the ultrasonic sensors from seeing the cable, the readings from each of the two ultrasonic sensors are pre-filtered based on both the variance of recent readings and the proximity of readings to the current altitude estimate, before being passed through a Kalman filter. The details of this pre-filtering are described in our previous work [5].

Now that we have an implementation system guided by simulation, we now discuss experimental validation in the field.

5 Field Experiments

In this section we describe the setup of field experiments and present results. To test our approach, we designed three field experiments: 1) a comparison of three methods of keeping a 3.5 *m* cable-connected sensor payload at a specified depth: air altimeter, ultrasonic altimeter, and depth altimeter; 2) step responses to changes in target depth for depth altimeter mode, and 3) an initial exploration of a longer, 8 *m* cable to test the limits of this approach.

All field experiments were conducted at Wildwood Lake near Lincoln, Nebraska, USA during March 2017, as shown in Figure 6 with a depth contour map. In total, we flew 33 missions during field experiments. The comparison dataset was collected during three days and the wind average speeds were 3.5 m/s, 2.0 m/s, and 1.3 m/s, respectively with maximum 5-second wind speed of 8.5 m/s, 7.2 m/s, and 7.9 m/s, respectively, indicating occasional strong gusts. We measured wind speed and direction using a weather station recording into a time-synced computer log.

5.1 Comparison of Flight Modes for Maintaining Constant Depth.

The purpose of this experiment is to compare three flight modes and quantify how precisely we can maintain the depth of a sensor payload. For more details about the three flight modes, please refer to Section 4.3.

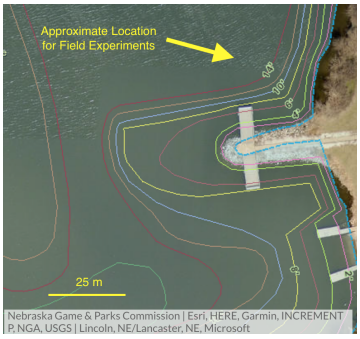

Fig. 6: Wildwood Lake, near Lincoln, Nebraska, USA, shown with depth contour (note: depth in feet).

We flew the vehicle from a shoreline jetty to a sampling location 10 m from shore, indicated in Figure 6, which permitted depth measurements to at least 4 m. For these experiments we used a 3.5 m cable affixed below the UAV's center of mass. For each mission we flew to the sampling location by human pilot and then would switch to computer control mode. Once switched into computer control mode, the system would attempt to hold the current pose. We repeated this experiment for each of the three modes (2 modes per flight, switching the order to avoid favoring one mode with stronger battery performance at the beginning of the flight) for a total of 12 minutes maintaining a specified depth for each mode. We use the depth altimeter reading as ground truth as it is accurate and fast as described in Section 4.2, and use this as a basis for evaluating the flight modes.

The results in Figure 7 show the distribution of target depth errors for three flight modes while attempting to maintain a constant depth. The data in the figure is collated from 3-4 flights per mode. We assume a Gaussian distribution of target errors and estimate the standard deviation, $\hat{\sigma}$ with Matlab's `normfit` function. As shown in the figure, the depth altimeter mode is much more precise than either ultrasonic or air pressure modes. Specifically, the statistical dispersion of depth readings in depth altimeter mode keeps 95% of readings within ± 8.4 $cm (\hat{\sigma} = 4.2$ $cm)$, two standard deviations from the target depth. This is within our goal of being able to obtain readings with a resolution of at least ≈ 25 cm. The ultrasonic-pressure altimeter mode shows $\hat{\sigma} = 16.1$ cm, or 95% of readings within ± 32.2 cm of the target depth, while the air altimeter has the largest dispersion, with 95% of readings within ± 60.2 cm $(\hat{\sigma} = 30.1$ $cm)$.

To better show the variation of depth readings in each mode, Figure 8 shows examples of 4 minutes of continuous flight holding a constant depth for each mode.

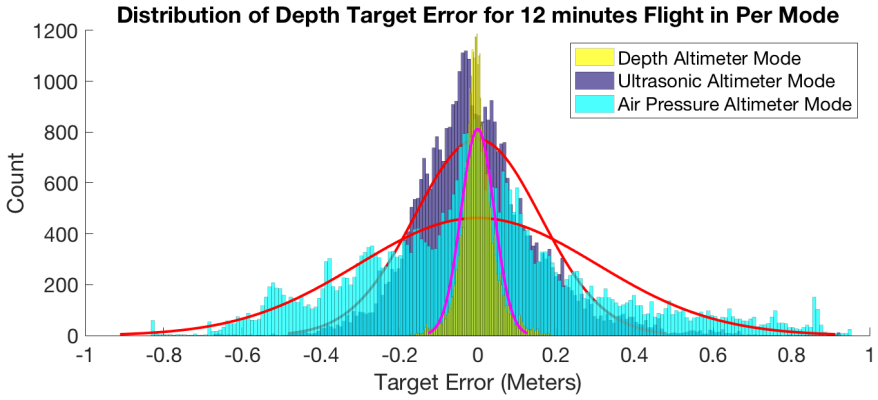

Fig. 7: Distribution of depth values when attempting to hold a constant depth during three flight modes.

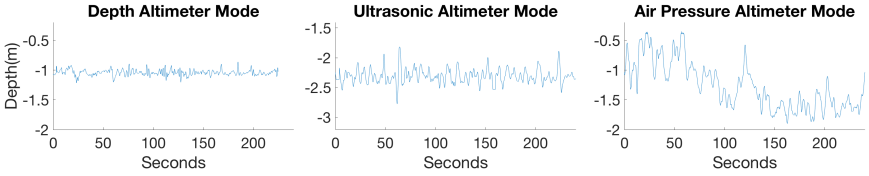

Fig. 8: Comparison of depth precision using three different flight modes. Note that the y-axes of all figures span 1.8 m.

As shown in Figure 8, depth altimeter mode stays closest to the target depth with almost no drift and small disturbances, and note than it maintained this target depth during 6 m/s gusty wind conditions. Also note in Figure 8 how ultrasonic altimeter mode is not as precise and occasionally deviates almost a meter, but does not drift significantly over time, unlike the air pressure altimeter mode. Notice that in air altimeter mode the depth readings can change by $30-40$ cm in a small amount of time, but that within 2 *minutes* the depth readings can be off by ± 0.75 m. The large drift in air pressure mode is likely caused by larger changes in ambient air pressure that occur frequently in windy conditions.

5.2 Step Response of Depth Altimeter Mode for a 3.5 m *Cable*

To determine if the system under depth altitude control could transition between target depth reference points, we conducted 'step response' maneuvers. Figure 9 shows the step responses under depth altimeter control. For each reference depth, we set the system to hold a particular depth, then commanded the computer control to adjust the reference depth by 0.5 m. Notice how the reference depths are repeatable both ascending and descending and the depth quickly settles to within ± 5 cm of the target depth. We used 0.5 m changes to avoid accelerating toward the water for

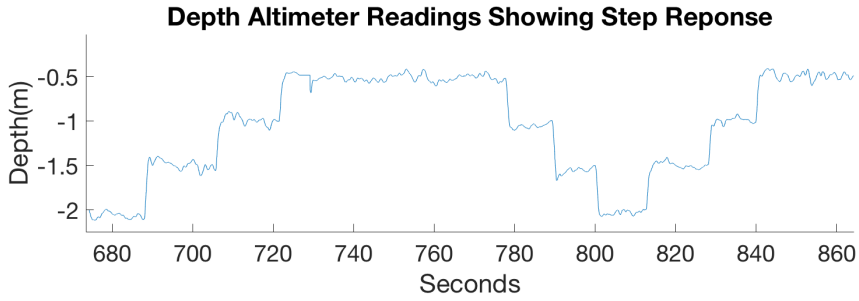

Fig. 9: Step response to target depths at 0.5 *m* increments for a 3.5 *m* cable.

longer than the human backup pilots were comfortable. This 0.5 *m* change in depth target is also within the range suggested during simulation (see Section 3.1) without implementing a descent velocity limit. We plan to test larger step responses after implementing additional overwater safety procedures, reserved for future work.

5.3 Longer 8 *m Cable: Target Error and Step Response*

As an additional experiment, we extended the cable length to 8 *m*. The reason we are interested in a longer cable is that in some applications we want to be able to measure water properties across a range of depths, nearly all < 10 *m*, and we also wanted to see what impact a longer cable would have on the ability of the depth altimeter to be a useful input to an altitude controller. Although simulation suggested that this approach should work for an 8 *m* cable, we thought the behavior of the long cable in both the air and the water was more complicated than what we could model. Therefore, we field tested the depth altimeter flight mode with the 8 *m* cable. The experimental setup for these tests is identical to those in Section 5 other than the cable length. We were only able to test the 8 *m* cable down to a depth of ≈ 4 *m*, due to depth and time limitations at our field location.

Figure 10 shows the results for holding a target depth, and for comparison the figure also shows the distribution of target errors for the 3.5 *m* cable depth altimeter experiments of Section 5.1. As shown in the figure, the 8 *m* cable is less precise than the 3.5 *m* cable, with 95% of readings within ± 14 $cm(\hat{\sigma} = 7.0cm)$, still close to the desired ≈ 0.25 *m* resolution. The dispersion of target errors for the 8 *m* cable still improves on the ultrasonic and air-pressure altimeter modes.

Figure 11 shows the system transitioning between target depths at 0.5 *m* increments. Like the previous results for the 3.5 *m* cable, the configuration with an 8 *m* cable can transition between target depths.

Because the 8 *m* cable allows the sensor payload to remain within ± 14 *cm* for nearly all readings, this means an 8 *m* cable is likely a viable method for monitoring water properties down to a depth of 7 *m*.

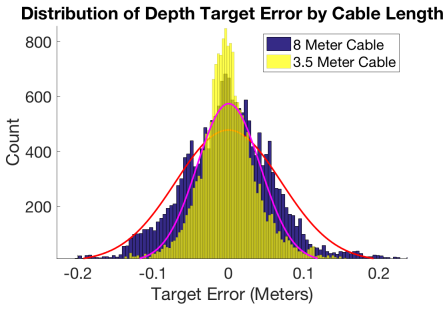

Fig. 10: 8 m cable : Distribution of Target Depth Errors for 4 *minutes* of Flight.

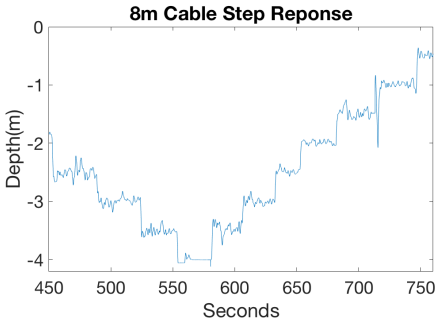

Fig. 11: 8 m cable : Step response to target depths at 0.5 m increments.

6 Discussion and Future Work

The depth precision for the depth altimeter flight mode exceeded our expectations, especially while flying in wind gusts at 80% of the manufacturer's limit of 10 m/s. We believe that any method for maintaining a specified depth not primarily based on the depth altimeter reading will fail to minimize the depth error in real-world conditions.

One future challenge includes integrating the sensor payloads requested by water scientists, and then validating the 'depth altitude' mode with a particular sensor payload. The challenge is that the sensors irregular shapes and configurations might result in different drag and terminal velocities. Also, devoting the majority of the payload to mass at the terminus of the cable can cause unstable flight dynamics. So far in our experiences, semi-rigid cables dampen much of the pendulum effect of slung loads for micro UAVs, but we have not tried scaling up slung payloads to much larger UAVs (5 kg payload) that might be useful for longer, deeper monitoring.

Fusing altitude and depth data might appear to be natural course, but currently we see little advantage to fusing information from other available sensors because they measure the altitude of the UAV, not the depth of the sensor payload, and the sampling frequency, accuracy, and precision of the depth altimeter make it easy to rely on. Instead of fusing data to form a depth estimate, we expect a hybrid controller could switch between flight modes based on heuristics of potentially dangerous behaviors (like hitting the bed below the water, becoming entangled, or getting encased in muck).

We examined the depth error as a function of lateral disturbance (error in x and y position), to test the idea that the depth error might increase when the vehicle is blown out of position by wind or by GPS drift. However, as predicted by the simulation in Section 3.1 we did not find a relationship between x and y error and depth error.

Flying over water with micro UAVs that are not waterproof is inherently risky, and there are a number of ways to increase the reliability of this kind of system:

1) better protection from unsafe descent, including conductivity sensors on the cable near the UAV, and at least one ultrasonic sensor for redundant backup; 2) buoy on a break-away cable; 3) fouling at the water's bottom might require mechanical design to protect the depth sensor from becoming coated in and fouled by the gelatinous goop lining many river and lake bottoms, perhaps mitigated by a second depth sensor higher up the cable; 4) buoyancy of the UAV.

7 Conclusions

This work explores a novel approach to maintaining and transitioning between precise depths for a submerged sensor payload passively cabled to a UAV. Our method enables the sensor payload to make 95% of sensor readings within ± 8.2 *cm* of the target depth, dramatically increasing the depth resolution of UAV-based water property datasets, even under gusty wind conditions. The non-linear dynamics of a system with a semi-rigid cable are challenging to model as it interacts with wind and water. Still, we used simulation to guide and refine our approach before implementation, and identified useful passive dynamics present during lateral disturbances that help keep the depth sensor on target. We presented a detailed description of the implementation and characterized the depth altimeter than enables our approach to maintain a precise depth. We conducted field experiments that validate the approach, resulting in a 75% reduction in standard deviation from a target depth when compared to the previous best method. We also presented initial results for a longer, 8 *m* cable, the longest cabled sensor system yet attempted in UAV-based water monitoring, and demonstrated that even an this length the approach allows water monitoring at precise depths from the air.

Acknowledgements We would like to commend Dr. Sebastian Elbaum and Dr. Justin Bradley for their insightful discussions regarding this approach. For help building the underwater sensor we thank Becca Horzewski. For help with field experiments we heartily thank Ajay Shankar, Ashraful Islam, Adam Plowcha, Chandima Fernando, and Nishant Sharma. This work was partially supported by NSF NRI-1638099, USDA-NIFA 2013-67021-20947 and USDA-NIFA 2017-67021-25924.

References

1. J. Higgins and C. Detweiler, "The waterbug sub-surface sampler: Design, control and analysis," in *Intelligent Robots and Systems (IROS), 2016 IEEE/RSJ International Conference on*. IEEE, 2016, pp. 330–337.
2. W. K. Dodds, W. W. Bouska, J. L. Eitzmann, T. J. Pilger, K. L. Pitts, A. J. Riley, J. T. Schloesser, and D. J. Thornbrugh, "Eutrophication of U.S. freshwaters: Analysis of potential economic damages," *Environmental Science & Technology*, vol. 43, no. 1, pp. 12–19, Jan. 2009.
3. I. Sanseverino, D. Conduto, P. POZZOLI, S. Dobricic, and T. Lettieri, "Algal bloom and its economic impact," *EUR 27905 EN; doi: 10.2788*, vol. 660478, 2016.

4. B. W. Brooks, J. M. Lazorchak, M. D. Howard, M.-V. V. Johnson, S. L. Morton, D. A. Perkins, E. D. Reavie, G. I. Scott, S. A. Smith, and J. A. Steevens, "Are harmful algal blooms becoming the greatest inland water quality threat to public health and aquatic ecosystems?" *Environmental Toxicology and Chemistry*, vol. 35, no. 1, pp. 6–13, 2016.
5. J.-P. Ore, S. Elbaum, A. Burgin, and C. Detweiler, "Autonomous aerial water sampling," *Journal of Field Robotics*, vol. 32, no. 8, pp. 1095–1113, 2015.
6. M. Chung, C. Detweiler, M. Hamilton, J. Higgins, J.-P. Ore, and S. Thompson, "Obtaining the thermal structure of lakes from the air," *Water*, vol. 7, no. 11, pp. 6467–6482, 2015.
7. M. Schwarzbach, M. Laiacker, M. Mulero-Pazmany, and K. Kondak, "Remote water sampling using flying robots," in *Unmanned Aircraft Systems (ICUAS), 2014 International Conference on*. IEEE, 2014, pp. 72–76.
8. P. Rodrigues, F. Marques, E. Pinto, R. Pombeiro, A. Lourenço, R. Mendonça, P. Santana, and J. Barata, "An open-source watertight unmanned aerial vehicle for water quality monitoring," in *OCEANS'15 MTS/IEEE Washington*. IEEE, 2015, pp. 1–6.
9. J. H. Bae, E. T. Matson, and B.-C. Min, "Towards an autonomous water monitoring system with an unmanned aerial and surface vehicle team," in *Safety, Security, and Rescue Robotics (SSRR), 2015 IEEE International Symposium on*. IEEE, 2015, pp. 1–2.
10. M. Ribeiro, A. S. Ferreira, P. Gonçalves, J. Galante, and J. B. de Sousa, "Quadcopter platforms for water sampling and sensor deployment," in *OCEANS 2016 MTS/IEEE Monterey*. IEEE, 2016, pp. 1–5.
11. A. DeMario, P. Lopez, E. Plewka, R. Wix, H. Xia, E. Zamora, D. Gessler, and A. P. Yalin, "Water plume temperature measurements by an unmanned aerial system (UAS)," *Sensors*, vol. 17, no. 2, p. 306, 2017.
12. D. Bershadsky, S. Haviland, P. E. Valdez, and E. Johnson, "Design considerations of submersible unmanned flying vehicle for communications and underwater sampling," in *OCEANS 2016 MTS/IEEE Monterey*. IEEE, 2016, pp. 1–8.
13. M. Dunbabin, A. Grinham, and J. Udy, "An autonomous surface vehicle for water quality monitoring," in *Proc. Australasian Conference on Robotics and Automation (ACRA)*, vol. 13, December 2009.
14. N. A. Cruz and A. C. Matos, "The MARES AUV, a modular autonomous robot for environment sampling," in *OCEANS 2008*. IEEE, 2008, pp. 1–6.
15. F. Zhang, O. En-Nasr, E. Litchman, and X. Tan, "Autonomous sampling of water columns using gliding robotic fish: Control algorithms and field experiments," in *Robotics and Automation (ICRA), 2015 IEEE International Conference on*. IEEE, 2015, pp. 517–522.
16. R. Eubank, E. Atkins, and D. Macy, "Autonomous guidance and control of the flying fish ocean surveillance platform," in *AIAA Infotech@ Aerospace Conference*, 2009, pp. 2009–2021.
17. S. Jain, S. Nuske, A. Chambers, L. Yoder, H. Cover, L. Chamberlain, S. Scherer, and S. Singh, "Autonomous river exploration," in *Field and Service Robotics*. Springer, 2015, pp. 93–106.
18. M. Burri, H. Oleynikova, M. W. Achtelik, and R. Siegwart, "Real-time visual-inertial mapping, re-localization and planning onboard mavs in unknown environments," in *Intelligent Robots and Systems (IROS), 2015 IEEE/RSJ International Conference on*. IEEE, 2015, pp. 1872–1878.
19. S. Tang and V. Kumar, "Mixed integer quadratic program trajectory generation for a quadrotor with a cable-suspended payload," in *Robotics and Automation (ICRA), 2015 IEEE International Conference on*. IEEE, 2015, pp. 2216–2222.
20. F. Goodarzi, D. Lee, T. Lee *et al.*, "Geometric stabilization of a quadrotor uav with a payload connected by flexible cable," in *American Control Conference (ACC), 2014*. IEEE, 2014, pp. 4925–4930.
21. R. Mahony, V. Kumar, and P. Corke, "Multirotor aerial vehicles: Modeling, estimation, and control of quadrotor," *IEEE Robotics & amp amp Automation Magazine*, no. 19, pp. 20–32, 2012.
22. "Pressure Sensor - MS5803-01BA," http://www.te.com/usa-en/product-CAT-BLPS0038.html, accessed: 2017-3-21.